This paper is available on line at http://www.mcponline.org

Myotubularin-related Proteins 3 and 4 Interact with Polo-like Kinase 1 and Centrosomal Protein of 55 kDa to Ensure Proper Abscission*[S]

Nicole St-Denis‡, Gagan D. Gupta‡, Zhen Yuan Lin‡, Beatriz Gonzalez-Badillo‡¶, Laurence Pelletier‡§, and Anne-Claude Gingras‡§‖

The myotubularins are a family of phosphatases that dephosphorylate the phosphatidylinositols phosphatidylinositol-3-phosphate and phosphatidylinositol-3,5-phosphate. Several family members are mutated in disease, yet the biological functions of the majority of myotubularins remain unknown. To gain insight into the roles of the individual enzymes, we have used affinity purification coupled to mass spectrometry to identify protein–protein interactions for the myotubularins. The myotubularin interactome comprises 66 high confidence (false discovery rate ≤1%) interactions, including 18 pairwise interactions between individual myotubularins. The results reveal a number of potential signaling contexts for this family of enzymes, including an intriguing, novel role for myotubularin-related protein 3 and myotubularin-related protein 4 in the regulation of abscission, the final step of mitosis in which the membrane bridge remaining between two daughter cells is cleaved. Both depletion and overexpression of either myotubularin-related protein 3 or myotubularin-related protein 4 result in abnormal midbody morphology and cytokinesis failure. Interestingly, myotubularin-related protein 3 and myotubularin-related protein 4 do not exert their effects through lipid regulation at the midbody, but regulate abscission during early mitosis, by interacting with the mitotic kinase polo-like kinase 1, and with centrosomal protein of 55 kDa (CEP55), an important regulator of abscission. Structure-function analysis reveals that, consistent with known intramyotubularin interactions, myotubularin-related protein 3 and myotubularin-related protein 4 interact through their respective coiled coil domains. The interaction between myotubularin-related protein 3 and polo-like kinase 1 relies on the divergent, nonlipid binding Fab1, YOTB, Vac1, and EEA1 domain of myotubularin-related protein 3, and myotubularin-related protein 4 interacts with CEP55 through a short GPPXXXY motif, analogous to endosomal sorting complex required for transport-I components. Disruption of any of these interactions results in abscission failure, by disrupting the proper recruitment of CEP55, and subsequently, of endosomal sorting complex required for transport-I, to the midbody. Our data suggest that myotubularin-related protein 3 and myotubularin-related protein 4 may act as a bridge between CEP55 and polo-like kinase 1, ensuring proper CEP55 phosphorylation and regulating CEP55 recruitment to the midbody. This work provides a novel role for myotubularin-related protein 3/4 heterodimers, and highlights the temporal and spatial complexity of the regulation of cytokinesis. ***Molecular & Cellular Proteomics 14: 10.1074/mcp.M114.046086, 946–960, 2015.***

The myotubularins are a subfamily of protein tyrosine phosphatases (PTPs)[1], consisting of sixteen conserved proteins. Despite containing the conserved $C(X)_5R$ catalytic motif found in all protein tyrosine phosphatases, myotubularins harbor active sites that do not dephosphorylate tyrosine, but instead catalyze the conversion of the phosphatidylinositol-type lipids

From the ‡Lunenfeld-Tanenbaum Research Institute, Mount Sinai Hospital, 600 University Avenue, Toronto, ON M5G 1X5, Canada; §Department of Molecular Genetics, University of Toronto, Toronto ON M5S 1A8, Canada

Received, November 3, 2014 and in revised form, January 22, 2015
Published, MCP Papers in Press, February 6, 2015, DOI 10.1074/mcp.M114.046086

Author contributions: N.S., G.D.G., L.P., and A.G. designed research; N.S., G.D.G., and Z.L. performed research; N.S. and B.G. contributed new reagents or analytic tools; N.S., G.D.G., and A.G. analyzed data; N.S. wrote the paper; L.P. supervised N.S. and G.D.G.; A.G. supervised N.S., Z.Y.L., and B.G.B.

[1] The abbreviations used are: PTP, protein tyrosine phosphatases; MTMR, myotubularin-related protein; SBF, SET binding factor; PI-phosphatidylinositol; PI3P, phosphatidylinositol-3-phosphate; PI5P, phosphatidylinositol-5-phosphate; PI3,5P, phosphatidylinositol-3,5-bisphosphate; AP-MS, affinity purification coupled to mass spectrometry; CEP55, centrosomal protein of 55 kDa; PLK1, polo-like kinase 1; ESCRT, endosomal sorting complex required for transport; RNAi, RNA interference; siRNA, small interfering RNA; HEK, human embryonic kidney; SAINT, significance analysis of interactome; PH-GRAM, pleckstrin homology-glucosyltransferases, Rab-like GTPase activators and myotubularins; protein tyrosine phosphatase; CC, coiled coil; FYVE, Fab1, YOTB, Vac1, and EEA1; Noc, nocodazole; Aph, aphidicolin; GFP/RFP, green/red fluorescent protein; PI3K, phosphatidylinositol 3-kinase; CDK, cyclin dependent kinase; ERK, extracellular signal-regulated kinase; FLAG, affinity tag, DYKDDDDK; HA, human influenza hemagglutinin affinity tag, YPYDVPDYA; kDa, kilodalton.

phosphatylinositol 3 phosphate (PI3P) and phosphatylinositol 3,5 phosphate (PI3,5P) to phosphatidylinositol (PI) and phosphatylinositol 5 phosphate (PI5P), respectively (1). Phosphatidylinositols are important molecules in a variety of processes, and as enzymatic regulators, myotubularins may function in cell proliferation, differentiation, survival, and cytoskeletal and junctional dynamics (1, 2). Of the sixteen myotubularins, only nine are active enzymes (supplemental Fig. S1*A*), as several lack catalytic cysteine residues (3). Myotubularins interact extensively with each other, and interactions between active and inactive pairs are frequent (4). It is thought that inactive myotubularins regulate the activity, substrate binding, and/or localization of their active binding partners (2).

Several myotubularins are linked to human disease. Myotubularin (MTM1), the first reported family member, is mutated in X-linked centronuclear myopathy (5), and Myotubularin related protein 14 (MTMR14) is mutated in autosomal centronuclear myopathy (6). Mutations in the active MTMR2 or its inactive binding partner, SET binding factor (SBF)2 (MTMR13), cause Charcot-Marie-Tooth diseases CMT4A and CMT4B, respectively (7–9). MTMR7 and MTMR9 have been associated with metabolic syndrome and obesity (MTMR9) (10, 11), epilepsy (MTMR7/9) (12), and Creutzfeldt-Jakob disease (MTMR7) (13). In addition, misregulation of the active phosphatase MTMR3 contributes to susceptibility to gastric and colon carcinomas (14), oral cancer (15), and lung cancer (16), and contributes to metastasis (15, 17). Aberrant expression of the inactive MTMR11 has been observed in acute myeloid leukemia (18), acute lymphocytic leukemia (19), and Her2-positive breast cancer (20). Generally, myotubularins are thought to integrate different cellular pathways, through both phosphatidylinositol regulation and protein–protein interactions (2). Despite their proposed involvement in a variety of cellular processes as well as disease states, many myotubularins remain poorly characterized, with their precise cellular functions not yet elucidated, and the pathological significance of those functions still unknown.

To gain insight on the biological functions of myotubularin family phosphatases, we have used affinity purification coupled to mass spectrometry (AP-MS) to identify protein–protein interactions for each myotubularin. The results expand upon the known repertoire of intra-myotubularin interactions, and, critically, identify specific novel interactions for individual myotubularins, providing valuable clues toward their respective functions. Further investigation revealed an unexpected role for MTMR3 and MTMR4 in abscission (21), the fission event at the end of cytokinesis that severs the final membrane link between divided daughter cells. Future studies of additional identified protein–protein interactions will undoubtedly illuminate the cellular roles of myotubularin family phosphatases.

EXPERIMENTAL PROCEDURES

Cloning—Each myotubularin was introduced into the Gateway entry vector pDONR223 (Life Technologies, Burlington, ON), and recombined into pDEST-pcDNA5-FRT-TO-3XFLAG (accession numbers for starting clones are listed in supplemental Table S1). MTMR3, MTMR4, PLK1, and CEP55 entry clones were transferred to pDEST-pcDNA5-FRT-TO-3XFLAG, pDEST-pcDNA5-FRT-TO-3XHA, and pDEST-pcDNA5-FRT-TO-GFP destination vectors. Point mutations (supplemental Table S1) were introduced into MTMR3 and MTMR4 entry clones using the Stratagene QuikChange Lightning Mutagenesis kit (Agilent Technologies, Santa Clara CA), and verified by DNA sequencing.

Cell Culture, Cell Cycle Treatments, RNAi, and Transfection—HEK293T, HeLa, and U-2 OS cells were maintained in standard media and conditions. Stable, tetracycline-inducible HEK293 T-REx and U-2 OS T-Rex cell lines were generated as previously described (22). For biochemical assays and MTMR3/4 overexpression analysis, protein expression was induced 24 h before harvest by addition of 1 μg/ml tetracycline (Tet). Transient transfection of plasmid DNA was performed using JetPrime (Polyplus-Transfection, New York, NY), and cells were harvested 24 h post-transfection. To arrest cells in S phase, 1.6 μg/ml aphidicolin (Sigma-Aldrich, Oakville, ON) was added to cells overnight. To arrest cells in prometaphase, aphidicolin was removed from cells with three PBS washes and cells were incubated overnight in the presence of 20 ng/ml nocodazole (Sigma-Aldrich). For certain experiments, nocodazole-arrested cells were incubated for 30 min with either 1 μM BI2536 (Selleck Chemicals, Houston, TX) or 10 μM RO-3306 (Sigma-Aldrich). To obtain cells later in mitosis, nocodazole-arrested cells were harvested by mitotic shake off, washed three times in PBS, and incubated in fresh media for the indicated times. For RNAi, cells were transfected by reverse transfection with siRNA (Dharmacon ON-TARGETplus, Lafayette, CO, supplemental Table S1) using Lipofectamine RNAiMax (Life Technologies). Cells were fed with fresh media 24 h after transfection, and harvested or fixed 72 h after RNA transfection. For rescue experiments, cells were induced 24 h after RNA transfection with 0.01 μg/ml Tet, and incubated an additional 48 h before fixation.

Affinity Purification and Mass Spectrometry—For each myotubularin and FLAG-GFP control, cell pellets from two 150-mm plates were lysed in 50 mM HEPES-KOH (pH 8.0), 100 mM KCl, 2 mM EDTA, 0.1% Nonidet P-40, and 10% glycerol and affinity-purified with M2-FLAG magnetic beads (Sigma-Aldrich), followed by on-bead trypsin digest as described (22). A spray tip was formed on fused silica capillary column (0.75 μm ID, 350 μm OD) using a laser puller (program = 4; heat = 280, FIL = 0, VEL = 18, DEL = 200). Ten centimeters ($\pm$ 1 cm) of C18 reversed-phase material (Reprosil-Pur 120 C18-AQ, 3 μm) was packed in the column by pressure bomb (in MeOH). The column was then pre-equilibrated in buffer A (6 μl) before being connected in-line to an Eksigent NanoLC-Ultra 2D plus HPLC system (AB-SCIEX, Concord, ON) coupled to a Thermo Electron LTQ-Orbitrap Velos (Thermo Scientific, Mississauga, ON) equipped with a Proxeon Biosystems nanoelectrospray ion source (Thermo Scientific). The LTQ-Orbitrap Velos instrument under Xcalibur 2.0 was operated in the data dependent mode to automatically switch between MS and up to 10 subsequent MS/MS acquisitions. Buffer A was 100% H_2O, 0.1% formic acid; buffer B was 100 ACN, 0.1% formic acid. The HPLC gradient program delivered an acetonitrile gradient over 125 min. For the first 20 minutes, the flow rate was 400 μl/min at 2% B. The flow rate was then reduced to 200 μl/min and the fraction of solvent B increased in a linear fashion to 35% until 95.5 min. Solvent B was then increased to 80% over 5 min and maintained at that level until 107 min. The mobile phase was then reduced to 2% B until the end of the run (125 min). The parameters for data depend-

ent acquisition on the mass spectrometer were: one centroid MS (mass range 400–2000) followed by MS/MS on the 10 most abundant ions. General parameters were: activation type = CID, isolation width = 1 *m/z*, normalized collision energy = 35, activation Q = 0.25, activation time = 10 msec. For data dependent acquisition, the minimum threshold was 500, the repeat count = 1, repeat duration = 30 s, exclusion size list = 500, exclusion duration = 30 s, exclusion mass width (by mass) = low 0.03, high 0.03.

Mass Spectrometry Data Extraction—RAW mass spectrometry files were converted to mzXML using ProteoWizard (3.0.4468; (23)) and analyzed using the iProphet pipeline (24) implemented within ProHits (25) as follows. The database consisted of the human and adenovirus complements of the RefSeq protein database (version 57) supplemented with "common contaminants" from the Max Planck Institute (http://maxquant.org/downloads.htm) and the Global Proteome Machine (GPM; http://www.thegpm.org/crap/index.html). The search database consisted of forward and reversed sequences (labeled "DECOY"); in total 72,226 entries were searched. The search engines used were Mascot (2.3.02; Matrix Science, Boston, MA) and Comet (2012.01 rev.3; (26), with trypsin specificity (two missed cleavages were allowed) and deamidation (NQ) and oxidation (M) as variable modifications. Charges +2, +3, and +4 were allowed, and the parent mass tolerance was set at 12 ppm, while the fragment bin tolerance was set at 0.6 amu. The resulting Comet and Mascot search results were individually processed by PeptideProphet (27), and peptides were assembled into proteins using parsimony rules first described in ProteinProphet (28) into a final iProphet protein output using the Trans-Proteomic Pipeline (TPP; Linux version, v0.0 Development trunk rev 0, Build 201303061711). TPP options were as follows: general options are -p0.05 -x20 -PPM -d"DECOY," iProphet options are -ipPRIME and PeptideProphet options are -OpdP. All proteins with a minimal iProphet protein probability of 0.05 were parsed to the relational module of ProHits. Note that for analysis with SAINT, only proteins with iProphet protein probability ≥0.95 are considered. This corresponds to an estimated protein-level FDR of ~0.5%. Furthermore, we required that each protein be detected by at least two unique peptides.

Interaction Scoring for FLAG AP-MS—For each bait, a cell line was prepared for mass spectrometric analysis as described above. Biological duplicates were grown/treated/processed at different times to maximize the variability and increase the robustness in the detection of true interactors. Negative control purifications (consisting of cells expressing GFP fused to the FLAG tag) were processed in parallel periodically throughout the data acquisition phase of the project in order to mitigate "batch effect" artifacts that we and others have reported (29). The quality of each sample was assessed manually by aligning the runs for the biological replicates in ProHits: samples of low quality were discarded, and other biological replicates were acquired. The main data set acquired in HEK293 Flp-In T-REx cells, and the smaller HeLa Flp-In T-REx data sets were analyzed separately with SAINTexpress (30), a computationally efficient reimplementation of the Significance Analysis of INTeractome method described previously (31). SAINT probabilities computed independently for each bait replicate are averaged, and the average probability (AvgP) is reported as the final SAINT score. To model the interactions robustly, the 35 HEK293-specific controls were first compressed to 25 "virtual controls" in which the 25 highest counts for each prey across all controls were used (see (32) for a description of this conservative scoring approach). Preys with AvgP ≥0.9 were considered "true" interactors (estimated FDR of 1%; see (33) for the description of the FDR estimation in SAINTexpress). For the HeLa cells, the six controls were compressed to four "virtual controls," and preys with AvgP ≥0.92 were considered "true" interactors at 1% FDR. Only trypsin and keratins were manually removed from this dataset after running SAINTexpress. The complete list of the interactions with scores is available in a searchable format on our website: http://prohits-web.lunenfeld.ca. Downloadable files and all raw mass spectrometry files are deposited in the MassIVE repository housed at the Center for Computational Mass Spectrometry at UCSD (http://proteomics.ucsd.edu/ProteoSAFe/datasets.jsp). The data set has been assigned the MassIVE ID MSV000078915 and is available for FTP download at: ftp://MSV000078915@massive.ucsd.edu. The data set was assigned the ProteomeXchange Consortium (http://proteomecentral.proteomexchange.org) identifier PXD001448. Visualization was performed using Cytoscape (34), or a custom dot plot mapping coded in R (35).

Cell Lysis, Co-Immunoprecipitation, SDS-PAGE, Western Blotting—Cells were washed with PBS and then lysed (50 mM HEPES-NaOH, pH 8.0, 100 mM KCl, 2 mM EDTA, 0.1% Nonidet P-40, 10% glycerol, 1 mM PMSF, 1 mM DTT, Sigma protease inhibitor mixture, P8340, 1:500, 40 mM β-glycerophosphate, 10 mM NaF, 0.3 mM sodium vanadate, and 100 nM okadiac acid) for 15 min on ice. Lysates were cleared by centrifugation for 20 min at 14,000 rpm at 4 °C. Lysates treated with λ phosphatase (New England Biolabs, Whitby, ON) were lysed without phosphatase inhibitors, and incubated with 400 U λ phosphatase in 1× Protein MetalloPhosphatase buffer (New England Biolabs) and 1 mM manganese chloride for 30 min at 30 °C. Cell lysates were boiled in Laemmli buffer for analysis by SDS-PAGE. After lysis of cells expressing FLAG-tagged proteins as above, cleared lysates were incubated with 5 μl of FLAG M2 magnetic beads (Sigma-Aldrich) with rotation for 1.5 h at 4 °C. Beads were washed twice in lysis buffer, and boiled in Laemmli sample buffer. Proteins were separated by electrophoresis on Criterion TGX 4–15% gradient gels (BioRad, Mississauga, ON), and then transferred to Protran nitrocellulose (GE Healthcare, Baie d'Urle, QC). Membranes were blocked in ddH_2O with 5% skim milk powder and incubated with primary and secondary antibodies (supplemental Table S1) in 50:50 PBS:LiCor Blocking Buffer (LiCor Biosciences, Lincoln, NE). Blots were washed in TBST, with a final wash in TBS. Antibody signals were visualized on a LiCor imaging system (LiCor Biosciences, Lincoln NE), with the exception of co-immunoprecipitated endogenous CEP55, which was incubated with a Donkey anti-mouse TrueBlot secondary conjugated to HRP (Rockland Immunochemicals, Limerick, PA; used to block the IgG heavy chain signal), and visualized using Lumiglo ECL (Cell Signaling Technologies, Danvers, MA).

Immunofluorescence, Fixed Imaging, Quantitative Imaging—Cells were seeded onto coverslips (Electron Microscopy Services, Hatfield, PA) or custom-made teflon printed coverslips (Scientific Devices Laboratory, Des Plaines, IL), and fixed with ice-cold methanol for 20 min at −20 °C. Samples were blocked in PBS with 2.5% BSA, and all antibodies (supplemental Table S1) were diluted in the same blocking buffer. Blocking, primary antibody, and secondary antibody incubations were performed for one hour at 37 °C, and coverslips were washed with PBS between incubations. DNA was counterstained with DAPI (Sigma), and the coverslips were mounted on glass slides by inverting them into mounting solution (ProLong Gold Antifade, Life Technologies). The samples were allowed to cure for 24–48 h. 3D deconvolution images were acquired on a DeltaVision Core imaging system (Applied Precision, Mississauga, ON) equipped with an IX71 microscope (Olympus, Richmond Hill, ON), CCD camera (CoolSNAP HQ2 1024 × 1024, Roper Scientific, Martinsried, Germany) and ×60/1.42 NA plan-Apochromat oil-immersion and 20× air objectives (Olympus). Z stacks (0.2 μm apart) were collected, deconvolved using softWoRx (v5.0, Applied Precision) and shown as maximum intensity projections (pixel size 0.1075 μm). Images were cropped in ImageJ (National Institutes of Health, Bethesda, MD). For all quantitatively compared images, identical imaging conditions (including exposure times) were used, and maximum intensity projections of Z-stacks

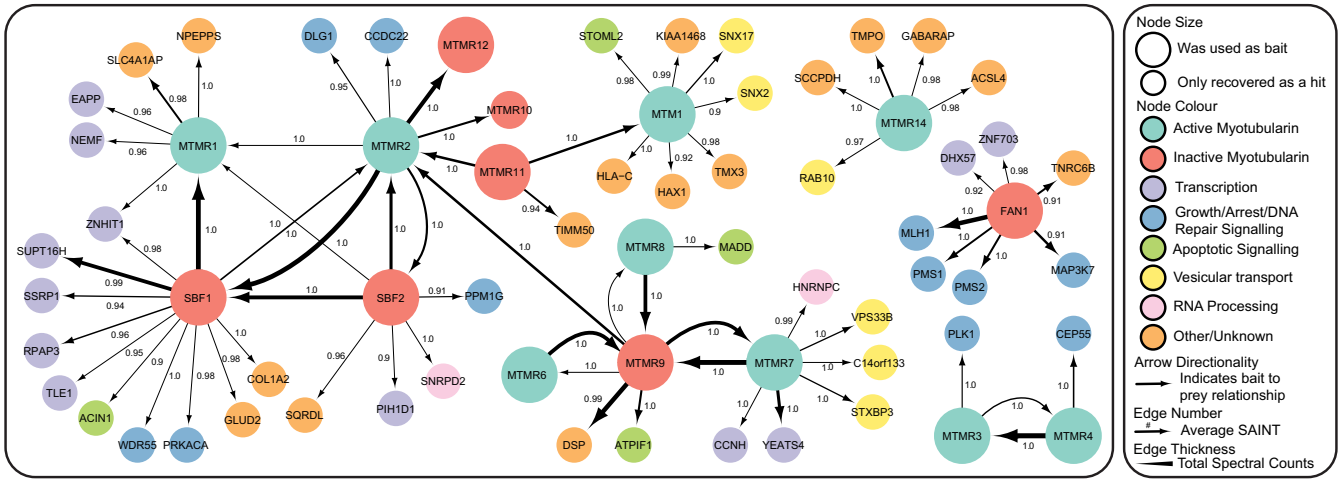

FIG. 1. **The myotubularin interactome.** Stable HEK293 Flp-In T-REx cell lines expressing FLAG-tagged versions of 15 human myotubularin-related proteins were generated, and protein interactions for each were identified by AP-MS. Two biological replicates were performed for each myotubularin, and compared with 18 FLAG-GFP controls. Statistical analysis was performed using SAINTexpress. All interactions shown had a false discovery rate (FDR) ≤1%.

were analyzed. Image quantitation was performed on unaltered projected Z-stacks using custom written MATLAB (MathWorks Inc., Natick, MA) scripts to mask the midbody regions and calculate integrated intensity for different markers.

Live Cell Imaging—HeLa cells with stable expression of either GFP-Tubulin and RFP-H2B, or GFP-CEP55 were transfected with control, MTMR3, MTMR4, or CEP55 RNA and plated in LabTek II imaging chambers (Thermo Scientific). Cells were fed with fresh media 24 h later, and arrested in G2 with 10 μM RO-3066 (Sigma) overnight. GFP-CEP55 cells were also transfected with mCherry-Tubulin (a kind gift from Geoffrey Hesketh) at the time of G2 arrest. Before imaging, the cells were released into mitosis by washing three times with PBS, and fed with phenol red-free DMEM supplemented with 10% FBS, 1 mM sodium pyruvate, and 1× Glutamax (all Life Technologies). Cells were imaged at 37 °C in 5% CO_2 at 60× magnification, with 2×2 binning. Image stacks of 24 μm were taken at 2 μm intervals, and 40 stage positions were imaged every 5 mins for 18 h. Exposure times were 100 ms each, at 10 and 32% transmission for GFP-Tubulin/GFP-CEP55 and H2B-RFP, respectively. Images were deconvolved and processed as above.

Statistical Methods—p values were obtained from two-tailed unpaired student t-tests. In the figures, * denotes $p < 0.05$, ** $p < 0.01$, and *** $p < 0.001$. In all box-whisker plots in Fig. 6, the red horizontal line denotes the mean, the pink box represents the 95% confidence interval, and the grayed region represents one standard deviation of the data.

RESULTS

Myotubularins Are Highly Interconnected, but Have Distinct Interaction Profiles—To shed light on possible functional roles for myotubularin family phosphatases, we performed AP-MS to identify protein–protein interactions for 15 of the myotubularins (MTMR10 was excluded because of low protein expression). We generated human embryonic kidney (HEK) 293 Flp-In T-REx cells stably expressing 3X-FLAG-tagged versions of each myotubularin, and performed FLAG immunoprecipitation on lysates from asynchronous cells. After on-bead trypsin digest, peptides were sequenced on a Velos Orbitrap mass spectrometer. Using the data from two independent biological replicates for each myotubularin, compared with 35 negative controls (3X-FLAG-GFP), we generated a probability score for each protein interaction using SAINTexpress (Significance Analysis of INTeractome) (30, 31). Generally, the myotubularins displayed a high degree of interconnectivity (Fig. 1, supplemental Tables S2 and S3, http://prohits-web.lunenfeld.ca). The majority of intra-family interactions in our dataset were between active and inactive members. The enzymes interact in several subclusters. For example, the active myotubularins MTMR1 and MTMR2, and inactive myotubularins SBF1 and SBF2, all interacted with each other, while each formed independent interactions with a variety of other proteins. The inactive enzymes MTMR9, 10, 11, and 12 sit on the periphery of this cluster, with all four forming interactions with the active phosphatase MTMR2. MTMR9 also interacted with three additional active myotubularins, MTMR6, 7, and 8, each of which displayed distinct interaction profiles. The intramyotubularin interactions were quite consistent with those previously determined by yeast two-hybrid (4) but also provided a few novel myotubularin–myotubularin interactions (supplemental Fig. S1*B*). Despite the interconnectivity of the majority of myotubularins, a few formed interactions outside of the main network, including the active myotubularin MTMR14 and inactive myotubularin FAN1 (MTMR15). Interestingly, MTMR14 and FAN1 are the only myotubularins that do not contain coiled coil domains, which are thought to mediate intramyotubularin interactions (36, 37). Dot plot analyses of all high-confidence interactions found for each myotubularin demonstrates that, outside of intra-myotubularin interactions, there was very little overlap in protein–protein interactions between myotubularins (supplemental Fig. S1*C*). This suggests that individual myotubularins have specialized functions, and the enzyme family may regulate a variety of cellular processes.

MTMR3 and MTMR4 Interact with PLK1 and CEP55—Similar to MTMR14 and FAN1, MTMR3 and MTMR4 formed interactions independently of the main myotubularin network. MTMR3 and MTMR4 formed clearly detectable reciprocal interactions by AP-MS. This is consistent with a previous yeast two-hybrid study, in which MTMR3 and MTMR4 were the only active myotubularins found to directly interact (4). In addition, MTMR3 interacted with the mitotic kinase PLK1, whereas MTMR4 interacted with CEP55, an important regulator of cytokinesis, the final stage of mitosis (38) (Fig. 1). To validate the interactions, we performed reciprocal AP-MS of PLK1 and CEP55. (Fig. 2*A*, supplemental Tables S2 and S3). PLK1 associated with a variety of proteins, including MTMR3 (for details on additional interacting proteins, see prohits-web.lunenfeld.ca). CEP55 interacted with several components of the ESCRT-I complex, and also interacted with MTMR4, although because of low spectral counts, this interaction was not significant. No PLK1 peptides were detected in CEP55 AP-MS, and vice versa. In addition, PLK1 peptides were only detected with MTMR3, and CEP55 peptides were only detected with MTMR4. The interactions were also observed after AP-MS of MTMR3, MTMR4, PLK1, and CEP55 in HeLa T-REx cell lines (supplemental Fig. S2*A*, supplemental Tables S4 and S5). To confirm the interactions between these proteins, we performed co-immunoprecipitation coupled to immunoblotting experiments. As expected, MTMR3 and MTMR4 established both homomeric and heteromeric interactions. However, in contrast to the apparent specificity of the MTMR3-PLK1 and MTMR4-CEP55 interactions in our mass spectrometry experiments, CEP55 and PLK1 recovered both myotubularins by co-immunoprecipitation/immunoblotting (Fig. 2*B*). The homo and heteromeric interactions and the interaction of both MTMR3 and 4 with PLK1 were also detected in U-2 OS cells (supplemental Fig. S2*B*; CEP55 was expressed at much lower levels in these cells, precluding conclusions as to its interactions with the myotubularins).

MTMR3 and MTMR4 Are Both Required for Cytokinesis—PLK1 is a master regulator of several stages of mitosis (27), including abscission. Chemical inhibition of PLK1 leads to cytokinesis defects, which include delays in cytokinesis and the formation of bi/multinucleated daughter cells (21). CEP55 is a crucial component of the spindle midbody, the microtubule-based structure that forms at the membrane bridge and coordinates abscission, and both depletion and overexpression of CEP55 results in abnormal midbody morphology and abscission defects, particularly the formation of bi- and multinucleated daughter cells upon mitotic exit (26). We therefore evaluated whether MTMR3 or MTMR4 are required for abscission. In both HeLa and U-2 OS cells, depletion of MTMR3, MTMR4 (supplemental Fig. S3*A* and S3*B*), or both myotubularins together led to levels of bi/multinucleated cells comparable to CEP55 depletion (Fig. 3*A*, supplemental Fig. S3*C*). Overexpression of MTMR3 or MTMR4 also resulted in significant binucleation (Fig. 3*B*), indicating that the levels of both

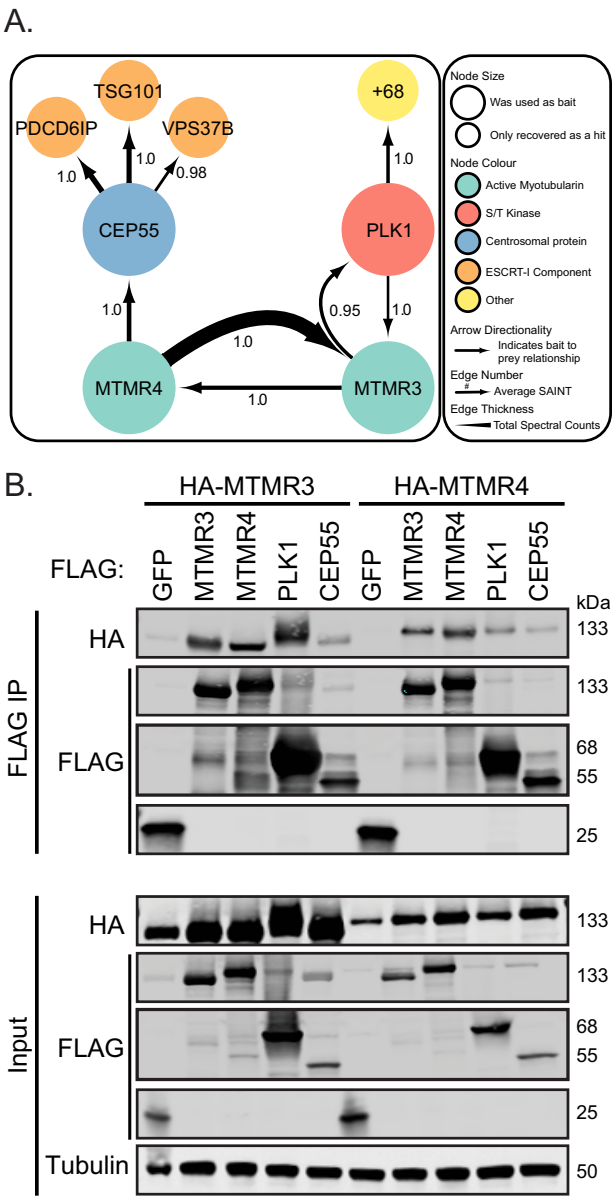

FIG. 2. **MTMR3 and MTMR4 interact with PLK1 and CEP55.** *A*, Stable HEK293 Flp-In T-REx cell lines expressing FLAG-tagged CEP55 or PLK1 were analyzed by AP-MS as in Fig. 1. Information on additional interactions can be found at prohits-web.lunenfeld.ca. *B*, HEK293T cells were transfected with HA-MTMR3 or HA-MTMR4, along with FLAG-tagged GFP, MTMR3, MTMR4, PLK1, and CEP55. After 24 h, cells were lysed and subjected to FLAG-immunoprecipitation. Western blot analysis using HA and FLAG antibodies were used to detect interactions between components.

myotubularins must be tightly regulated to ensure proper abscission. With the exception of small but significant increases in binucleation upon depletion of MTMR7 and MTMR9 (3.9% ($p = 0.0305$) and 3.5% ($p = 0.0427$), respectively), none of the other myotubularins affected binucleation (Fig. 3*C*). The mild phenotype of MTMR7 and MTMR9 in our assay was not because of inefficient silencing as MTMR7 and MTMR9 were depleted to comparable levels as MTMR3

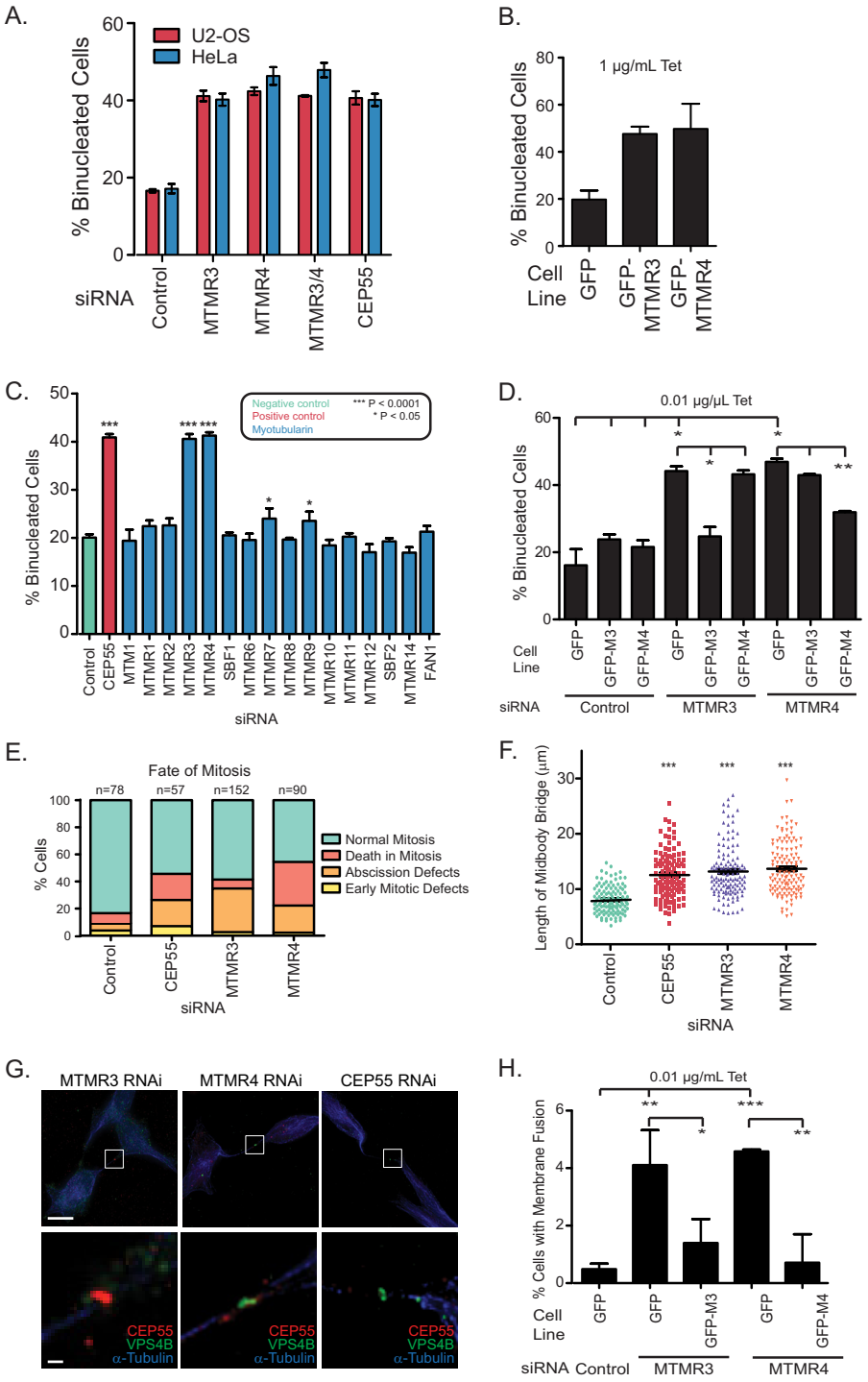

FIG. 3. **MTMR3 and MTMR4 are both required for abscission.** *A*, HeLa and U-2 OS cells were treated with siRNA against MTMR3, MTMR4, both myotubularins together, or CEP55. After 72 h, cells were fixed, stained with α-Tubulin antibody and DAPI, and analyzed for binucleation. *B*, U-2 OS Flp-In T-REx cells stably expressing FLAG-tagged GFP, GFP-MTMR3, or GFP-MTMR4 were induced with 1 µg/ml tetracycline, fixed and stained 72 h later, and analyzed for binucleation. *C*, HeLa cells were transfected with siRNA targeting each of the 16 myotubularins, and incubated 72 h before fixation and staining. *D*, Stable U-2 OS cell lines with inducible expression of FLAG-GFP, siRNA-resistant GFP-MTMR3, or siRNA-resistant GFP-MTMR4 were transfected with control, MTMR3, or MTMR4 siRNA. Twenty-four hours later protein expression was induced with 0.01 µg/ml tetracycline (note the decreased tetracycline added to the medium to prevent the overexpression effects observed in Fig. 3*B*). Cells were fixed and stained 48 h later, and analyzed for abscission defects. *E*, Fate of mitosis of HeLa cells depleted of CEP55, MTMR3, or MTMR4 was assayed by live cell imaging 48 h after siRNA transfection. The number of mitoses analyzed for each condition (*n*) is indicated. *F*, The lengths of the microtubule midbody bridge in cytokinetic HeLa cells depleted of CEP55, MTMR3, or MTMR4 were measured. At least 100 midbodies were measured per condition. *G*, Postmitotic cells with continued membrane attachment after MTMR3, MTMR4, or CEP55 depletion are shown, stained for α-Tubulin to visualize interphase microtubules, CEP55, and the ESCRT-III cofactor VPS4B. Scale bars: 10 µm (full images), 2 µm (zoomed images). *H*, U-2 OS Flp-In T-REx cells were treated as in *D*, and assessed for the presence of postmitotic membrane fusions. Results for all binucleation assays, as well as the membrane fusion assay, are the average of three biological replicates, with least 300 cells were analyzed per treatment for each replicate.

and MTMR4 (supplemental Fig. S3*D*), and unlike MTMR3 and MTMR4, overexpression of MTMR7 nor MTMR9 resulted in increased binucleation (supplemental Fig. S3*E*). These experiments confirm that the observed phenotype is specific to MTMR3 and MTMR4 (with approximately double the number of binucleated cells; both $p < 0.0001$), and is not a general consequence of myotubularin loss (for example, through global changes in phospholipid levels). The increased number of binucleated cells upon depletion of MTMR3 or MTMR4 was rescued by expression of respective siRNA-resistant variants, indicating that the defects are not caused by off-target effects (Fig. 3*D*; Note that 0.01 µg/ml tetracycline was used to induce a lower amount of MTMR3 and MTMR4 in rescue experiments, as induction with 1 µg/ml tetracycline resulted in an overexpression phenotype). By contrast, GFP-MTMR3 was not able to rescue the MTMR4 siRNA phenotype, or vice

versa. This suggests that MTMR3 and MTMR4 functions are not interchangeable, and are both required to ensure genomic integrity in daughter cells.

Binucleation in daughter cells does not necessarily indicate problems in abscission, as issues with either chromosome segregation in anaphase or cleavage furrow ingression in telophase can also produce this phenotype (39). Therefore, we performed live cell imaging in HeLa cells expressing both GFP-Tubulin and H2B-RFP. In cells depleted of either MTMR3 or MTMR4, chromosome segregation and cleavage furrow ingression occurred normally (supplemental Fig. S3*F*, supplemental Movies S1–S3), but cells displayed a variety of mitotic phenotypes. In addition to forming binucleated daughter cells, many cells died, during cytokinesis, and, in the case of already-binucleated cells, during subsequent early mitosis (Fig. 3*E*).

The spindle midbody is a highly organized structure, and depletion of CEP55 results in abscission failure because of the formation of disorganized, nonfunctional midbodies (40). As with CEP55, depletion of MTMR3 or MTMR4 resulted in significantly longer midbody microtubule bridges (13.1 μm and 13.6 μm, respectively, compared with 7.94 μm for control cells; Fig. 3*F*). Postmitosis, the abnormal membrane fusions remaining between daughter cells after MTMR3/4 depletion contained disorganized midbody components, suggesting that these bridges were the remnants of nonfunctional midbodies (Fig. 3*G*). The presence of these membrane fusions was rescued upon expression of siRNA-resistant MTMR3 and MTMR4 (Fig. 3*H*). Taken together, these observations suggest that loss of either MTMR3 or MTMR4 results in abscission defects caused by aberrant midbody formation.

The Roles of MTMR3 and MTMR4 in Abscission are Lipid Independent—Recently, it has been demonstrated that correct PI3P concentration at the midbody is crucial for proper abscission, as depletion of PI3 kinase components VPS34 or BECN1 results in abscission failure (41). However, whether PI3P phosphatases are involved in the regulation of abscission has not been investigated. MTMR3 and MTMR4 are both active enzymes, with demonstrated phosphatase activity against both PI3P and PI3,5P (42, 43). As both CEP55 and PLK1 localize to the midbody (38), we postulated that interaction with PLK1 and CEP55 may serve to recruit MTMR3 and/or MTMR4 to the midbody, where they might regulate midbody PI3P concentration. Despite the ability to rescue the loss of MTMR3 or MTMR4 function in abscission (Fig. 3*D*), we noted that neither GFP-MTMR3 nor GFP-MTMR4 visibly colocalized with CEP55 at the spindle midbody (Fig. 4*A*; note that, like others in the field (4), we have not found suitable antibodies for the detection of endogenous MTMR3 and MTMR4 by immunofluorescence). However, it is possible that a small, undetectable fraction of the proteins could localize to the midbody and affect PI3P concentration. Therefore, to further investigate this possibility, we performed rescue experiments with mutants of MTMR3 and MTMR4.

MTMR3 and MTMR4, like other myotubularins, contain both a PH-GRAM phosphatidylinositol-binding domain, and a specialized protein tyrosine phosphatase (PTP) domain that dephosphorylates phosphatidylinositols (Fig. 4*B*, 4*C*). In addition (and unique across the myotubularin family), MTMR3 and MTMR4 also contain phosphatidylinositol-binding FYVE domains. The FYVE domain of MTMR4 is responsible for its localization to endosomes in interphase cells (44). The MTMR3 FYVE domain, however, is divergent in sequence from most FYVE domains, does not bind phosphatidylinositols or localize MTMR3 to endosomes, and is therefore considered nonfunctional (45). To assess whether the lipid binding and/or phosphatase activities of MTMR3 or MTMR4 were required for their cytokinetic functions, function-disrupting point mutations were introduced in each of the conserved domains. Phosphatase-dead versions (PTPmut, C413S for MTMR3, C407S for MTMR4 (44, 46)) and FYVE domain-inactive mutants (MTMR3-FYVEmut, C1174S (46), MTMR4-FYVEmut, C1169S (4)) have been previously described. Point mutations to disrupt lipid-binding through the PH-GRAM domains (PHmut, L73P for both enzymes) target a conserved residue which, when mutated, abrogates the lipid-binding of the MTM1 PH-GRAM domain (47). GFP-tagged, siRNA-resistant forms of each mutant protein were evaluated for the ability to rescue MTMR3/MTMR4 RNAi-induced binucleation in U-2 OS T-REx stable cell lines (Fig. 4*B*, 4*C*). Importantly, expression of each MTMR3/4 mutant was comparable to the wild-type proteins (Fig. 4*D*), and all mutants were expressed as full-length fusion proteins (supplemental Fig. S4). Phosphatase-dead versions (PTPmut) of both enzymes rescued RNAi-induced binucleation, indicating that lipid phosphatase activity is not required for proper abscission (this also rules out a hypothetical protein target for MTMR3/4 phosphatase activity). In addition, abscission occurred normally upon disruption of the PH-GRAM domain (PHmut) of either phosphatase, or the FYVE domain of MTMR4 (MTMR4-FYVEmut), indicating that lipid binding ability is also not required for abscission. Curiously, disruption of the MTMR3 FYVE domain (MTMR3-FYVEmut), which does not bind lipids (45) failed to rescue MTMR3 RNAi-induced binucleation, suggesting that it may play a (lipid-independent) role in regulating abscission. As none of the conserved domains known to bind phospholipids were required to rescue abscission defects caused by MTMR3/4 depletion, the roles of MTMR3 and MTMR4 in abscission appear to be lipid-independent.

PLK1/MTMR3/MTMR4/CEP55 Interactions Are Required for Proper Cytokinesis—In addition to various lipid-binding domains, myotubularins typically contain a coiled coil domain, which mediates the formation of myotubularin dimers (36, 37). We used MultiCoil (48) to identify important hydrophobic residues in the coiled coil regions of MTMR3 and MTMR4, and mutated these to proline to disrupt coiled coil structure (MTMR3-CCmut, V1049/L1052/L1056P, MTMR4-CCmut, V1036/L1039/V1043/L1046P). Expression of MTMR4-CCmut

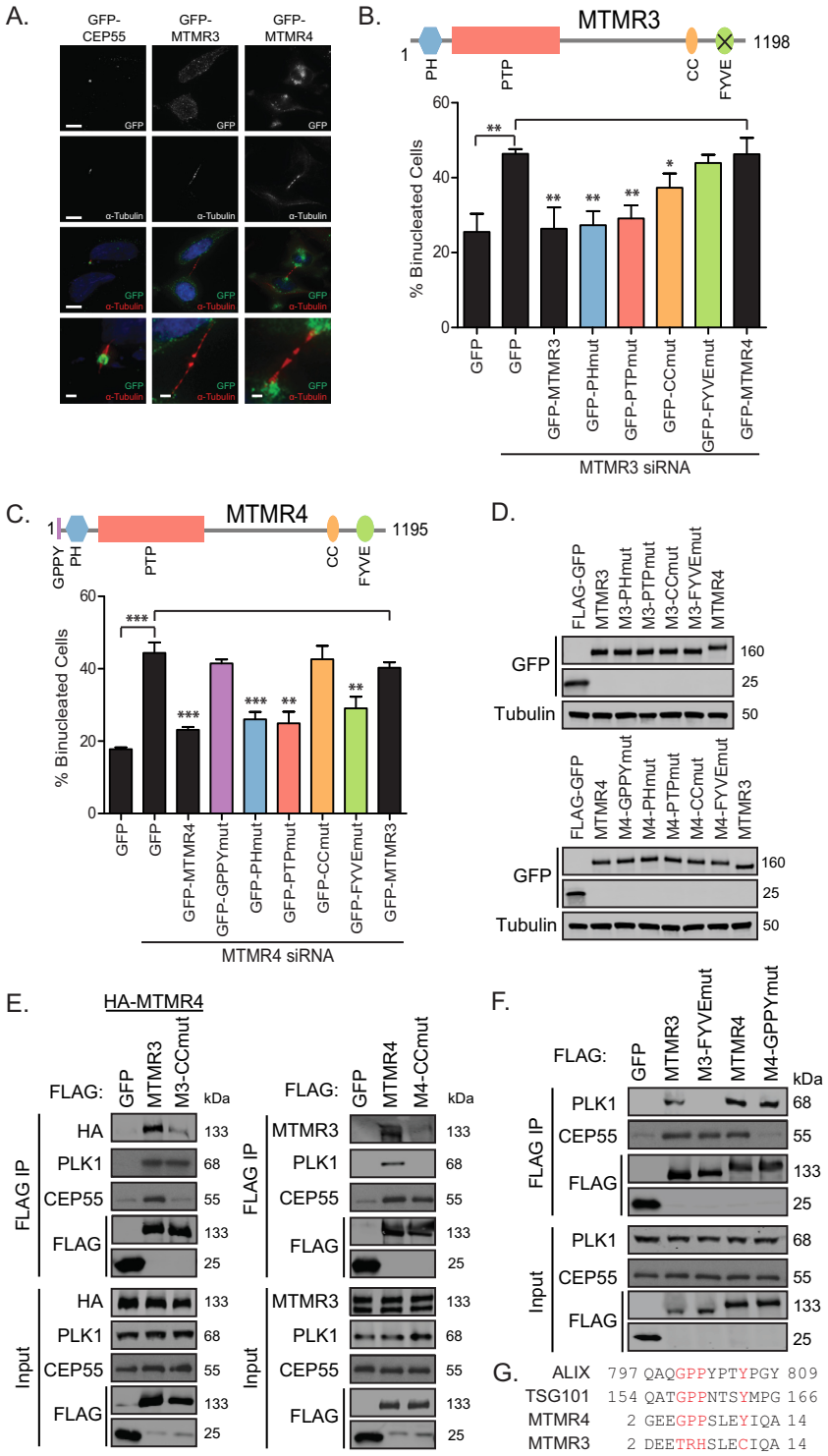

FIG. 4. **Proper abscission does not require MTMR3/MTMR4 lipid phosphatase activity, but does require interactions between MTMR3, MTMR4, PLK1, and CEP55.** *A*, U-2 OS Flp-In T-REx cell lines with inducible expression of GFP-tagged CEP55, MTMR3, or MTMR4 were fixed and immunostained with GFP and α-Tubulin antibodies. Scale bars: 10 μm (full images), 2 μm (zoomed images). *B*, Schematic of MTMR3 functional domains. The black X in the MTMR3 FYVE domain denotes its inability to bind phospholipids. U-2 OS Flp-In T-REx cell lines with inducible expression of siRNA-resistant, GFP-tagged MTMR3 were transfected with either control or MTMR3 siRNA and incubated 24 h before protein expression was induced with 0.01 μg/ml tetracycline. 72 h after RNA transfection, cells were fixed and stained for α-Tubulin and GFP, and analyzed for abscission defects. *C*, Schematic of MTMR4 functional domains. U-2 OS Flp-In T-REx cell lines with inducible expression of siRNA-resistant, GFP-tagged MTMR4 lines were analyzed as in panel *B*. For *B* and *C*, three biological replicates were performed,

failed to rescue the binucleation observed upon depletion (Fig. 4*C*), and expression of MTMR3-CCmut partially rescued the phenotype, with a 9% decrease in binucleation ($p = 0.0173$) (Fig. 4*B*). Disruption of the coiled coil domain of either myotubularin disrupted the MTMR3-MTMR4 interaction (Fig. 4*E*). In addition, although disruption of the MTMR3 coiled coil domain did not affect the interaction between MTMR3 and PLK1, it did decrease the interaction between MTMR3 and CEP55, implying that the MTMR3-MTMR4 interaction is required for MTMR3 and CEP55 to associate. Similarly, disruption of the MTMR4 coiled coil domain affected the MTMR4-PLK1 interaction, but not the MTMR4-CEP55 interaction, suggesting that MTMR4-PLK1 interactions are dependent on the presence of MTMR3.

Because MTMR3-FYVEmut could not rescue MTMR3 RNAi-induced binucleation (Fig. 4*B*), we investigated whether it may also be involved in association with its binding partners. MTMR3-FYVEmut co-immunoprecipitated less PLK1 than wild-type MTMR3, but had no effect on the amount of co-immunoprecipitated CEP55 (Fig. 4*F*), suggesting that the role of the MTMR3 FYVE domain may be to facilitate interaction with PLK1. The interaction between CEP55 and the ESCRT-I components ALIX and TSG101 is dependent on the presence of a GPPXXXY (where X is any amino acid) motif in the ESCRT-I components (49). Interestingly, such a motif is also located at the extreme N terminus of MTMR4, but is not present in the MTMR3 N terminus (Fig. 4*G*) or in any of the other myotubularins. Mutating this motif (MTMR4-GPPYmut, Y11A) resulted in failure to rescue MTMR4 RNAi-induced binucleation (Fig. 4*C*). This mutant also failed to interact with CEP55, confirming that MTMR4 interacts with CEP55 in a manner similar to the ESCRT-I/CEP55 interactions. However, the interaction between MTMR4 and PLK1 was maintained in the presence of this mutation (Fig. 4*F*). Taken together, these results suggest that the PLK1-MTMR3, MTMR3-MTMR4, and MTMR4-CEP55 interactions occur through different binding interfaces, and, as disruption of any of these binding interfaces failed to rescue RNAi-induced abscission defects, we conclude that interactions between PLK1, MTMR3, MTMR4, and CEP55 are required for proper abscission.

Phosphorylated MTMR3 and MTMR4 Interact with PLK1 and CEP55 During Early Mitosis—Mutation of the coiled coil domains of either MTMR3 or MTMR4 resulted not only in loss of the MTMR3-MTMR4 interaction, but also affected interactions with PLK1 and CEP55 (Fig. 4*E*), implying that the MTMR3-MTMR4 heterodimer may act as a bridge to facilitate additional interactions. To investigate this possibility, we performed immunoprecipitation experiments after depletion of either MTMR3 or MTMR4, and assayed interactions with PLK1 and CEP55. Upon depletion of MTMR4, FLAG-MTMR3 copurified less CEP55, but not less PLK1, than in the presence of MTMR4 (Fig. 5*A*). Conversely, upon MTMR3 depletion, FLAG-MTMR4 showed decreased interaction with PLK1, but not CEP55 (Fig. 5*B*). Taken together with the mutant experiments in Fig. 4*E* and 4*F*, we propose associations between PLK1, MTMR3, MTMR4, and CEP55, in which MTMR3 and MTMR4 dimerize via their respective coiled coil domains, MTMR4 interacts with CEP55 through its N-terminal GPPY motif, analogous to ESCRT-I components, and MTMR3 relies on its non-lipid binding FYVE domain to interact with PLK1.

The results above suggest that interactions between MTMR3, MTMR4, PLK1, and CEP55 are required for proper cytokinesis, yet unlike CEP55 and PLK1, MTMR3, and MTMR4 do not localize to the midbody. To determine if these interactions were regulated in a cell cycle-dependent manner, cells expressing FLAG-MTMR4 were synchronized first in S phase with aphidicolin, then released into G2 and arrested in prometaphase with nocodazole. Cells were released from nocodazole arrest and harvested at intervals afterward. Synchronization was monitored by blotting for phospho-histone 3 serine 10 in the lysates; note that, as expected (50, 51), PLK1 total levels were lowest in aphidicolin-arrested cells and highest in nocodazole arrested cells. FLAG-MTMR4 was immunoprecipitated to assay interactions with MTMR3, PLK1, and CEP55. No change was observed in MTMR3-MTMR4 interaction through the cell cycle, suggesting that at least a portion of the two myotubularins may interact constitutively. However, the interactions between MTMR4 and both CEP55 and PLK1 were strongest in prometaphase lysates, and were lost as cells progressed through mitosis (Fig. 5*C*). Intriguingly, PLK1 has been reported to phosphorylate CEP55 during early mitosis, preventing early recruitment of CEP55 to the developing midbody (21). This suggests that the interactions reported here may play a role in regulating PLK1 phosphorylation of CEP55.

and at least 300 cells were counted per sample in each replicate. *D*, U-2 OS Flp-In T-REx cell lines with inducible expression of siRNA-resistant, GFP-tagged MTMR3 or MTMR4 point mutations were subjected to Western blot analysis. For MTMR3, mutations are as follows: PHmut, L73P; PTPmut, C413S; CCmut, V1049/L1052/L1056P; FYVEmut, C1174S. For MTMR4, GPPYmut, Y11A; PHmut, L73P; PTPmut, C407S; CCmut, V1036/L1039/V1043/L1046P; FYVEmut, C1169S. PH, PH-GRAM; PTP, protein tyrosine phosphatase; CC, coiled coil; FYVE, FYVE domain; GPPY, GPPXXXY motif. *E*, HEK293T cells were transfected with FLAG-tagged wild type or coiled coil mutant versions of MTMR3 or MTMR4, and lysed after 24 h. Because of the lack of MTMR4 antibodies, HA-MTMR4 was cotransfected in the MTMR3 experiment. FLAG immunoprecipitation was performed, and interactions with indicated components were analyzed by Western blot. *F*, HEK293T cells were transfected with FLAG-tagged wild-type MTMR3, MTMR3-FYVEmut, wild-type MTMR4, or MTMR4-GPPYmut, and lysed after 24 h. FLAG immunoprecipitation was performed, and interactions with PLK1 and CEP55 were analyzed by Western blot. kDa, kilodalton. *G*, Sequence alignment of ALIX, TSG101, and MTMR4 GPPY motifs. MTMR3 does not contain an analogous sequence. Flanking numbers indicate the amino acid positions of the motif in each protein.

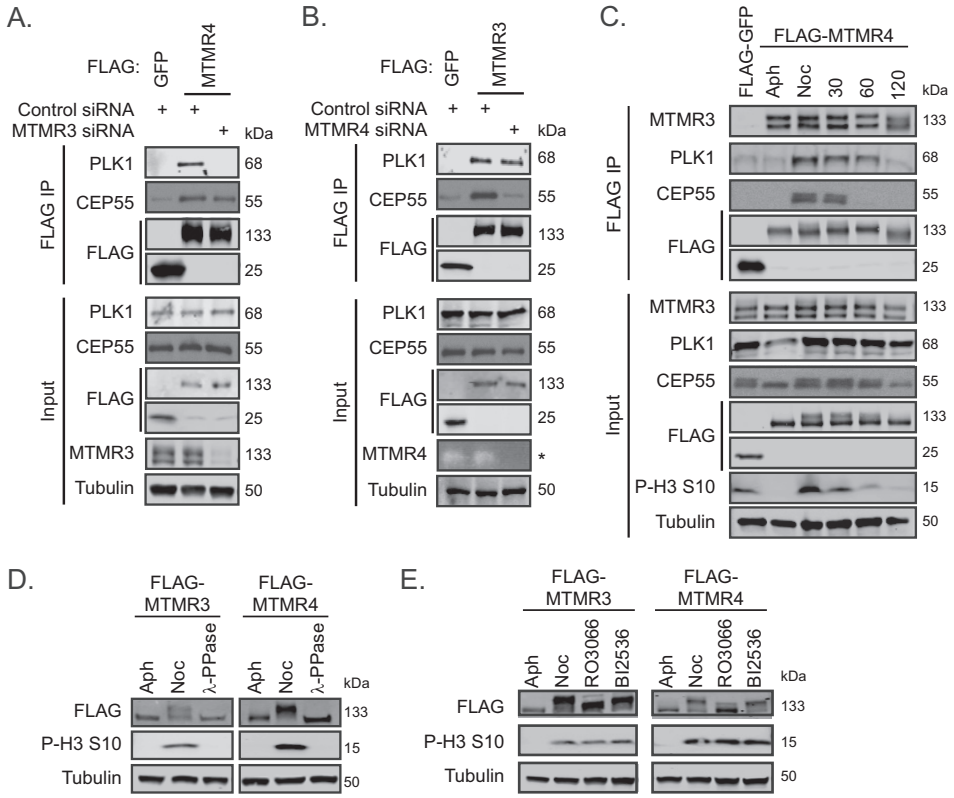

FIG. 5. **MTMR3/MTMR4 heterodimers associate with PLK1 and CEP55 during early mitosis.** *A*, HEK293 Flp-In T-REx cells were transfected with either control or MTMR3 siRNA for 48 h before induction of FLAG-MTMR4 expression for 24 h. Lysates were subjected to FLAG immunoprecipitation and immunoblotted for complex components. *B*, HEK293 Flp-In T-REx cells were transfected with either control or MTMR4 siRNA for 48 h before induction of FLAG-MTMR4 expression for 24 h. Lysates were subjected to FLAG immunoprecipitation and immunoblotted for complex components. MTMR4 depletion was confirmed by RT-PCR (denoted by *). *C*, HEK293T cells were transfected with FLAG-MTMR4, and synchronized in various stages of the cell cycle. Lysates were FLAG-immunoprecipitated, and MTMR3, PLK1, and CEP55 interactions were analyzed by Western blot. Cell cycle progression was monitored by immunoblotting the input lysates for phosphorylated serine 10 of Histone H3 (P-H3 S10). Aph, aphidicolin; Noc, nocodazole; kDa, kilodalton. *D*, HeLa Flp-In T-REx cells with stable expression of either FLAG-MTMR3 or FLAG-MTMR4 were arrested in either S phase or mitosis. Mitotic lysates were then incubated with or without λ phosphatase before Western blot analysis. *E*, Stable HeLa Flp-In T-REx cell lines were arrested as in *D*, and mitotic cells were incubated with either 10 μM RO-3066 or 1 μM BI2536 for 30 min before lysis and Western blot analysis.

We also observed that FLAG-MTMR4 undergoes a mobility shift in mitotic lysates (Fig. 5*C*). In addition, HA-MTMR3 undergoes a similar shift upon co-expression of PLK1 (see Fig. 2*B*). This may suggest that MTMR3 and MTMR4 are phosphorylated during mitosis, potentially by PLK1. To confirm that these mobility shifts are indeed the result of phosphorylation, lysates from stable HeLa lines expressing either FLAG-MTMR3 or FLAG-MTMR4 were arrested in either S phase or mitosis as above. As shown in Fig. 5*D*, both MTMR3 and MTMR4 displayed mobility shifts in cells arrested in prometaphase. When mitotic lysates were treated with λ phosphatase, the mobility shifts were lost, confirming that MTMR3 and MTMR4 are phosphorylated in early mitosis. To assess the impact of PLK1 on these phosphorylation events, mitotic cells were incubated with BI2536, an inhibitor of PLK1. Interestingly, we observed little to no change in MTMR3 or MTMR4 mobility shifts upon PLK1 inhibition (Fig. 5*E*). In contrast, inhibition of CDK1 decreased both mobility shifts dramatically, suggesting that the mitotic phosphorylation of MTMR3 and MTMR4 depends not on PLK1 activity, but on CDK1 activity.

MTMR3 and MTMR4 Regulate CEP55 Recruitment to the Midbody—CEP55 is a crucial component of the midbody, and is required for the subsequent sequential recruitment of first ESCRT-I and then ESCRT-III, which is responsible for the severing of the membrane link between the newly-formed daughter cells (52–54). Because aberrant recruitment of CEP55 to the midbody results in abscission failure (21), we investigated whether depletion of MTMR3 or MTMR4 affected the recruitment of CEP55 to the midbody. Quantitative imaging of CEP55 demonstrates that upon depletion of MTMR3, CEP55 intensity at the midbody increases ~eightfold ($p = 1.6982*10^{-20}$) (Fig. 6*A*). This increase in CEP55 intensity may correlate with early recruitment of CEP55 to the midbody during telophase in MTMR3 RNAi-treated cells (Fig. 6*B*), similarly to loss of CEP55 phosphorylation by PLK1 (21). To

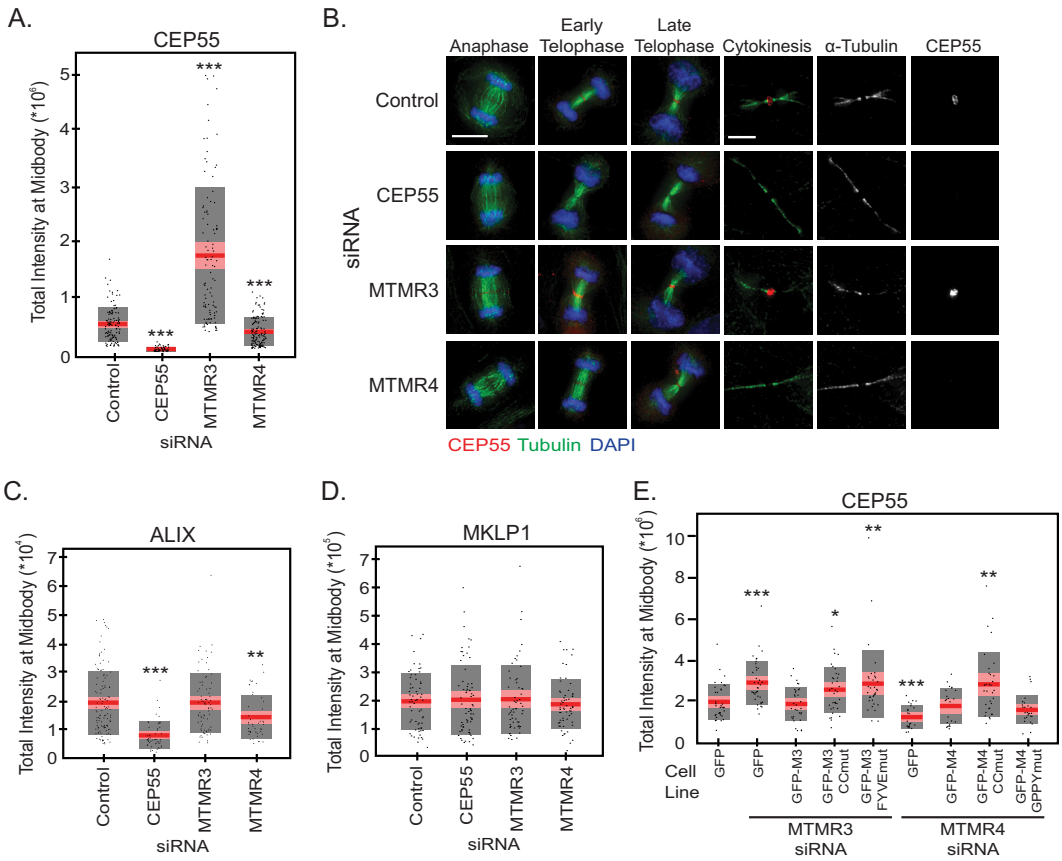

FIG. 6. **MTMR3 and MTMR4 regulate CEP55 recruitment to the midbody.** *A*, HeLa cells depleted of CEP55, MTMR3, or MTMR4 for 72 h were fixed and immunostained with antibodies against CEP55, α-Tubulin, and PLK1. Midbodies were imaged quantitatively and the total CEP55 intensity at the midbody was measured. *B*, Fixed images of CEP55 recruitment to the central spindle/midbody through late mitosis after depletion of CEP55, MTMR3, or MTMR4. Scale bars: 10 μm. *C*, *D*, HeLa cells were treated as in *B*, but stained with antibodies against the ESCRT-I component ALIX or the Centralspindalin component MKLP1. E. Stable U-2 OS cell lines with inducible expression of FLAG-GFP or siRNA-resistant forms of GFP-MTMR3 and GFP-MTMR4 were transfected with the indicated siRNAs and incubated 24 h before protein expression was induced with 0.01 μg/ml tetracycline. 48 h after induction, cells were fixed and stained for α-Tubulin, GFP, and CEP55. Midbodies were imaged quantitatively, and total CEP55 intensity at the midbody was measured. For all quantitative imaging experiments, results shown depict one of three independent replicates, with at least 60 midbodies measured per condition per replicate. The red line indicates the mean, the pink box indicates the 95% confidence interval, and the gray box indicates one standard deviation.

investigate this further, we performed live cell imaging in HeLa cells expressing GFP-CEP55 and mCherry-Tubulin (supplemental Fig. S5, supplemental Movies S4–S6). Live cell imaging confirmed that depletion of MTMR3 resulted in increased CEP55 at the midbody, however, we were unable to conclusively show that this was because of early recruitment of CEP55. Intriguingly, MTMR4 depletion had the opposite effect, as CEP55 intensity at the midbody was significantly decreased compared with control cells (37% reduction; $p = 9.8*10^{-5}$) (Fig. 6*A*). Importantly, changes in CEP55 intensity at the midbody were not caused by changes in total CEP55 protein level upon depletion of MTMR3 or MTMR4 (supplemental Fig. S3*A*).

As CEP55 is required for the recruitment of ESCRT-I components to the midbody (49), we next investigated whether ESCRT-I recruitment to the midbody was similarly affected by MTMR3/4 depletion. As expected, given the decreased amount of CEP55 present at the midbody, depletion of MTMR4 also resulted in a significant decrease (~35%) in ALIX intensity at the midbody ($p = 0.0055$) (Fig. 6*C*). However, despite the large increase in CEP55 intensity at the midbody after MTMR3 depletion, ALIX intensity was comparable to control cells, suggesting that loss of MTMR3 is not sufficient to deregulate ALIX levels at the midbody. To ensure that the recruitment defects observed upon MTMR3/4 depletion were caused by misregulation of CEP55, and not general defects in midbody formation, we also quantitated the midbody intensity of MKLP1, a component of the central spindalin complex, which is recruited before CEP55 (40). As expected, depletion of neither MTMR3 nor MTMR4 (nor CEP55) affected the amount of MKLP1 at the midbody (Fig. 6*D*).

Finally, to confirm that interactions between MTMR3, MTMR4, PLK1, and CEP55 are crucial for proper CEP55

recruitment to the midbody, we examined whether expression of siRNA-resistant MTMR3/4 containing interaction-disrupting point mutants (MTMR3-CCmut, MTMR3-FYVEmut, MTMR4-CCmut, and MTMR4-GPPYmut) could rescue aberrant CEP55 recruitment to the midbody. Consistent with their inability to rescue abscission defects, expression of GFP-MTMR3-CCmut and GFP-MTMR3-FYVEmut (which cannot bind MTMR4 and PLK1, respectively) did not resolve the increased CEP55 intensity observed with MTMR3 depletion ($p = 0.014$ and 0.0064, respectively, compared with control CEP55 intensity), whereas expression of wild-type GFP-MTMR3 returned CEP55 levels to control levels (Fig. 6*E*). Expression of wild-type GFP-MTMR4 returned CEP55 intensity to control levels, whereas expression of GFP-MTMR4-GPPYmut (which cannot bind CEP55) resulted in only partial rescue of the decreased CEP55 intensity observed with MTMR4 depletion (~15% lower than control levels, $p = 0.06$). On the other hand, expression of GFP-MTMR4-CCmut (which cannot bind MTMR3 or PLK1) reversed the phenotype, resulting in increased CEP55 intensity at the midbody ($p = 0.0068$), as is observed with MTMR3 depletion and PLK1 inhibition. From this, we conclude these interactions may occur to ensure continued phosphorylation of CEP55 by PLK1 during early mitosis, leading to proper temporal recruitment of appropriate amounts of CEP55, and subsequently ESCRT components, to the midbody.

DISCUSSION

In this study, we have systematically identified protein–protein interactions established by a relatively understudied family of protein phosphatases, the myotubularins. Consistent with previous studies, the myotubularins displayed extensive intra-family interactions, yet the protein–protein interactions made by each enzyme outside the family were quite divergent, suggesting that each myotubularin may have unique roles in the cell. Consistent with roles in membrane trafficking, a few myotubularins associated with transport proteins, including MTM1 with the sorting nexins SNX2 and SNX17, and MTMR7 with VPS33B, and the VPS33B-interacting protein C14orf133 (also known as VIPAS39). Several myotubularins also interacted with cellular signaling proteins, including several involved in the regulation of growth, DNA repair, and cell death. Even more striking, however, were the many interactions made with transcriptional regulators. This included interactions between the inactive myotubularin SBF1 and both components of the FACT complex (SSRP1 and SUPT16H), which acts in transcriptional elongation and, along with protein kinase CK2, regulates p53 after UV-induced DNA damage (55, 56). Several other SBF1 interactors also interact with p53 and/or CK2, including WDR55 (57), TLE1 (58), and ZNHIT1 (which also significantly interacts with MTMR1) (59), suggesting that MTMR1/SBF1-containing complexes may play a role in p53-mediated transcriptional responses to DNA damage. One of the products of myotubularin dephosphorylation, PI5P, was recently demonstrated to affect transcription in *Arabidopsis thaliana*, by binding to the transcriptional regulator ATX1 (60), but to our knowledge this is the first indication that animal myotubularins may regulate transcription.

We chose to further investigate some intriguing interactions found between MTMR3, MTMR4, PLK1, and CEP55, and discovered important roles for MTMR3 and MTMR4 in abscission. Taken together, our data support a model in which MTMR3 and MTMR4 form interactions with CEP55 and PLK1 during early mitosis that regulate CEP55 recruitment to the midbody. It will be important to validate these interactions using the endogenous proteins, once suitable antibodies are available. It is tempting to speculate that these interactions participate in the regulation of PLK1-mediated phosphorylation of CEP55. For example, an MTMR3-MTMR4 scaffold could explain how PLK1 is recruited to CEP55. PLK1 typically forms phospho-dependent interactions with substrates via its polo box domain (61). In early mitosis, phospho-binding sites on PLK1 substrates are generally formed through CDK1 phosphorylation. Although there are two CDK1 sites just upstream of the CEP55 PLK1 site, neither site conforms to the consensus requirements for polo box domain binding (62, 63). In addition, despite a documented direct kinase-substrate relationship, no study has successfully copurified CEP55 and PLK1 (supplemental Tables S2–S5, (21)). If the MTMR3/4 heterodimer acts as a scaffold, a functional polo box domain binding site in CEP55 would be unnecessary. It will be important to experimentally test this hypothesis.

Along with forming a heterodimeric scaffold with MTMR3, it appears that MTMR4 may play an additional role in CEP55 regulation. With loss of MTMR4, MTMR3 and PLK1 would not be recruited to CEP55, and therefore CEP55 should not be phosphorylated, and should display increased midbody intensity. However, depletion of MTMR4 actually decreased CEP55 recruitment to the midbody (Fig. 5*C*), suggesting that the effect of MTMR4 depletion is dominant over the phenotypic effects of either MTMR3 depletion or PLK1 inhibition. The exact mechanism behind this effect is unknown, but the CEP55-MTMR4 interaction does appear important for proper CEP55 recruitment. As MTMR4 interacts with CEP55 using a short peptide motif analogous to one in ESCRT-I components ALIX and TSG101 (49), it is possible that MTMR4 competes with ESCRT-I for CEP55 binding. This would explain why loss of MTMR3 results in increased CEP55 at the midbody without a corresponding increase in ESCRT-I: with MTMR3 depletion, MTMR4 would still interact with CEP55, presumably blocking increased CEP55-ESCRT-I interactions.

MTMR3 and MTMR4 may represent two novel examples of interphase membrane trafficking proteins that are co-opted for “mitotic moonlighting” functions (50). During interphase, MTMR4 is primarily localized to early endosomes, where it regulates sorting of endosomal cargo (44), while MTMR3 remains in the cytoplasm (4), and has been implicated in the regulation of autophagy (48) and cell migration (49). These

functions—which unlike abscission, all involve the regulation of phosphatidylinositol levels—are presumably not required during mitosis, when endosomal fusion and recycling are reduced (51, 52), autophagy is strongly inhibited (53), and the cytoskeleton is drastically reorganized, precluding migration. This raises the possibility that other myotubularins may have mitotic and/or lipid-independent functions, possibly involving a subset of the interactions identified in this study. The switch controlling MTMR3/MTMR4 function may involve phosphorylation. In this study, we have demonstrated that both myotubularins are phosphorylated during mitosis (Fig. 5*D*), and this phosphorylation is dependent on CDK1 activity (Fig. 5*E*). Accordingly, both proteins contain potential CDK1 sites (but no clear PLK1 consensus sequences, consistent with the lack of effects observed with PLK1 inhibition). Identification of these phosphorylation sites, as well as examination of their impact on both PLK1/MTMR3/MTMR4/CEP55 interactions and regulation of abscission, will be important in the future to determine if this is indeed the mechanistic switch that diverts MTMR3 and MTMR4 from their interphase roles.

Mitosis is a tightly regulated process with several distinct steps, all of which need to occur properly to ensure genomic integrity in the resultant daughter cells. Defects in abscission, the final step in mitosis, cause aneuploidy that can result in tumorigenesis (64–66). Both PLK1 and CEP55 have transforming abilities and are overexpressed in a variety of cancers (67–70), and given the importance of each protein in coordinating abscission, overexpression of either could dramatically accelerate genomic instability. It is possible cells evolved to use MTMR3 and MTMR4 as intermediates linking PLK1 to CEP55 (as opposed to direct binding between CEP55 and the PLK1 polo box domain) as a buffer, ensuring that abscission is not drastically affected by changes in PLK1 activity or CEP55 expression. If so, disruption of these interactions might be a useful therapeutic means of increasing cancer cell death, as the survival of cancer cells depends on maintaining an optimal level of genomic instability (71).

Acknowledgments—We thank Jianping Zhang and Guomin Liu for prohits-web.lunenfeld.ca website design and maintenance, Brett Larsen and Monika Tucholska for expert advice on mass spectrometry experiments, and Francis Barr, Daniel Gerlich, Harald Stenmark, Otis Vacratsis, Fred Robinson, Christina Mitchell, and Geoffrey Hesketh for the kind gift of reagents.

* This work was supported by the Government of Canada through the Canadian Institutes of Health Research (A.-C.G.; MOP-84314; to L.P.; MOP-123468) and Genome Canada and the Ontario Genomics Institute (OGI-069 to A.-C.G.), the US National Institutes of Health (to A.-C.G; 5R01GM94231), and by the generous support of the Krembil Foundation (to L.P.). A.-C.G. is the Canada Research Chair in Functional Proteomics and the Lea Reichmann Chair in Cancer Proteomics. L.P. is the Canada Research Chair in Centrosome Biogenesis and Function. N.S. is supported by a postdoctoral fellowship from the Canadian Institutes of Health Research.

S This article contains supplemental Figs. S1 to S5, Tables S1 to S5, and Movies S1 to S6.

¶ Current address: Batchelor Children's Institute, Miller School of Medicine, University of Miami, Miami, FL, USA 33136

‖ To whom correspondence should be addressed: Lunenfeld-Tanenbaum Research Institute, Mount Sinai Hospital, 600 University Avenue, Toronto, ON M5G 1X5, Canada. Tel.: 416-596-5027; Fax: 416-586-8869; E-mail: gingras@lunenfeld.ca.

REFERENCES

1. Robinson, F. L., and Dixon, J. E. (2006) Myotubularin phosphatases: policing 3-phosphoinositides. *Trends Cell Biol.* **16,** 403–412
2. Hnia, K., Vaccari, I., Bolino, A., and Laporte, J. (2012) Myotubularin phosphoinositide phosphatases: cellular functions and disease pathophysiology. *Trends Mol. Med.* **18,** 317–327
3. Alonso, A., Sasin, J., Bottini, N., Friedberg, I., Friedberg, I., Osterman, A., Godzik, A., Hunter, T., Dixon, J., and Mustelin, T. (2004) Protein tyrosine phosphatases in the human genome. *Cell* **117,** 699–711
4. Lorenzo, O., Urbé, S., and Clague, M. J. (2006) Systematic analysis of myotubularins: heteromeric interactions, subcellular localization, and endosome related functions. *J. Cell Sci.* **119,** 2953–2959
5. Dang, H., Li, Z., Skolnik, E. Y., and Fares, H. (2004) Disease-related myotubularins function in endocytic traffic in Caenorhabditis elegans. *Mol. Biol. Cell* **15,** 189–196
6. Tosch, V., Rohde, H. M., Tronchère, H., Zanoteli, E., Monroy, N., Kretz, C., Dondaine, N., Payrastre, B., Mandel, J. L., and Laporte, J. (2006) A novel PtdIns3P and PtdIns(3,5)P2 phosphatase with an inactivating variant in centronuclear myopathy. *Hum. Mol. Genet.* **15,** 3098–3106
7. Bolino, A., Muglia, M., Conforti, F. L., LeGuern, E., Salih, M. A., Georgiou, D. M., Christodoulou, K., Hausmanowa-Petrusewicz, I., Mandich, P., Schenone, A., Gambardella, A., Bono, F., Quattrone, A., Devoto, M., and Monaco, A. P. (2000) Charcot-Marie-Tooth type 4B is caused by mutations in the gene encoding myotubularin-related protein-2. *Nat. Genet.* **25,** 17–19
8. Azzedine, H., Bolino, A., Taïeb, T., Birouk, N., Di Duca, M., Bouhouche, A., Benamou, S., Mrabet, A., Hammadouche, T., Chkili, T., Gouider, R., Ravazzolo, R., Brice, A., Laporte, J., and LeGuern, E. (2003) Mutations in MTMR13, a new pseudophosphatase homolog of MTMR2 and Sbf1, in two families with an autosomal recessive demyelinating form of Charcot-Marie-Tooth disease associated with early-onset glaucoma. *Am. J. Hum. Genet.* **72,** 1141–1153
9. Senderek, J., Bergmann, C., Weber, S., Ketelsen, U. P., Schorle, H., Rudnik-Schöneborn, S., Büttner, R., Buchheim, E., and Zerres, K. (2003) Mutation of the SBF2 gene, encoding a novel member of the myotubularin family, in Charcot-Marie-Tooth neuropathy type 4B2/11p15. *Hum. Mol. Genet.* **12,** 349–356
10. Yanagiya, T., Tanabe, A., Iida, A., Saito, S., Sekine, A., Takahashi, A., Tsunoda, T., Kamohara, S., Nakata, Y., Kotani, K., Komatsu, R., Itoh, N., Mineo, I., Wada, J., Masuzaki, H., Yoneda, M., Nakajima, A., Miyazaki, S., Tokunaga, K., Kawamoto, M., Funahashi, T., Hamaguchi, K., Tanaka, K., Yamada, K., Hanafusa, T., Oikawa, S., Yoshimatsu, H., Nakao, K., Sakata, T., Matsuzawa, Y., Kamatani, N., Nakamura, Y., and Hotta, K. (2007) Association of single-nucleotide polymorphisms in MTMR9 gene with obesity. *Hum. Mol. Genet.* **16,** 3017–3026
11. Hotta, K., Kitamoto, T., Kitamoto, A., Mizusawa, S., Matsuo, T., Nakata, Y., Kamohara, S., Miyatake, N., Kotani, K., Komatsu, R., Itoh, N., Mineo, I., Wada, J., Yoneda, M., Nakajima, A., Funahashi, T., Miyazaki, S., Tokunaga, K., Masuzaki, H., Ueno, T., Hamaguchi, K., Tanaka, K., Yamada, K., Hanafusa, T., Oikawa, S., Yoshimatsu, H., Sakata, T., Matsuzawa, Y., Nakao, K., and Sekine, A. (2011) Association of variations in the FTO, SCG3, and MTMR9 genes with metabolic syndrome in a Japanese population. *J. Hum. Genet.* **56,** 647–651
12. Baulac, S., Gourfinkel-An, I., Couarch, P., Depienne, C., Kaminska, A., Dulac, O., Baulac, M., LeGuern, E., and Nabbout, R. (2008) A novel locus for generalized epilepsy with febrile seizures plus in French families. *Arch. Neurol.* **65,** 943–951
13. Sanchez-Juan, P., Bishop, M. T., Aulchenko, Y. S., Brandel, J.-P., Rivadeneira, F., Struchalin, M., Lambert, J.-C., Amouyel, P., Combarros, O., Sainz, J., Carracedo, A., Uitterlinden, A. G., Hofman, A., Zerr, I., Kretzschmar, H. A., Laplanche, J.-L., Knight, R. S. G., Will, R. G., and van Duijn, C. M. (2012) Genome-wide study links MTMR7 gene to variant Creutzfeldt-Jakob risk. *Neurobiol. Aging* **33,** 1487.e21–28

14. Song, S. Y., Kang, M. R., Yoo, N. J., and Lee, S. H. (2010) Mutational analysis of mononucleotide repeats in dual specificity tyrosine phosphatase genes in gastric and colon carcinomas with microsatellite instability. *APMIS* **118,** 389–393
15. Kuo, Y. Z., Tai, Y. H., Lo, H. I., Chen, Y. L., Cheng, H. C., Fang, W. Y., Lin, S. H., Yang, C. L., Tsai, S. T., and Wu, L. W. (2014) MiR-99a exerts anti-metastasis through inhibiting myotubularin-related protein 3 expression in oral cancer. *Oral Dis.* **20,** e65–75
16. Hu, Z., Wu, C., Shi, Y., Guo, H., Zhao, X., Yin, Z., Yang, L., Dai, J., Hu, L., Tan, W., Li, Z., Deng, Q., Wang, J., Wu, W., Jin, G., Jiang, Y., Yu, D., Zhou, G., Chen, H., Guan, P., Chen, Y., Shu, Y., Xu, L., Liu, X., Liu, L., Xu, P., Han, B., Bai, C., Zhao, Y., Zhang, H., Yan, Y., Ma, H., Chen, J., Chu, M., Lu, F., Zhang, Z., Chen, F., Wang, X., Jin, L., Lu, J., Zhou, B., Lu, D., Wu, T., Lin, D., and Shen, H. (2011) A genome-wide association study identifies two new lung cancer susceptibility loci at 13q12.12 and 22q12.2 in Han Chinese. *Nat. Genet.* **43,** 792–796
17. Oppelt, A., Haugsten, E. M., Zech, T., Danielsen, H. E., Sveen, A., Lobert, V. H., Skotheim, R. I., and Wesche, J. (2014) PIKfyve, MTMR3 and their product PtdIns5P regulate cancer cell migration and invasion through activation of Rac1. *Biochem. J.* **461,** 383–390
18. Kabir, N. N., Rönnstrand, L., and Kazi, J. U. (2013) Deregulation of protein phosphatase expression in acute myeloid leukemia. *Med. Oncol.* **30,** 517
19. La Starza, R., Crescenzi, B., Pierini, V., Romoli, S., Gorello, P., Brandimarte, L., Matteucci, C., Kropp, M. G., Barba, G., Martelli, M. F., and Mecucci, C. (2007) A common 93-kb duplicated DNA sequence at 1q21.2 in acute lymphoblastic leukemia and Burkitt lymphoma. *Cancer Genet. Cytogenet.* **175,** 73–76
20. Lucci, M. A., Orlandi, R., Triulzi, T., Tagliabue, E., Balsari, A., and Villa-Moruzzi, E. (2010) Expression profile of tyrosine phosphatases in HER2 breast cancer cells and tumors. *Cell Oncol.* **32,** 361–372
21. Bastos, R. N., and Barr, F. A. (2010) Plk1 negatively regulates Cep55 recruitment to the midbody to ensure orderly abscission. *J. Cell Biol.* **191,** 751–760
22. Kean, M. J., Couzens, A. L., and Gingras, A. C. (2012) Mass spectrometry approaches to study mammalian kinase and phosphatase associated proteins. *Methods* **57,** 400–408
23. Kessner, D., Chambers, M., Burke, R., Agus, D., and Mallick, P. (2008) ProteoWizard: open source software for rapid proteomics tools development. *Bioinformatics* **24,** 2534–2536
24. Shteynberg, D., Deutsch, E. W., Lam, H., Eng, J. K., Sun, Z., Tasman, N., Mendoza, L., Moritz, R. L., Aebersold, R., and Nesvizhskii, A. I. (2011) iProphet: multi-level integrative analysis of shotgun proteomic data improves peptide and protein identification rates and error estimates. *Mol. Cell. Proteomics* **10,** M111.007690
25. Liu, G., Zhang, J., Larsen, B., Stark, C., Breitkreutz, A., Lin, Z. Y., Breitkreutz, B. J., Ding, Y., Colwill, K., Pasculescu, A., Pawson, T., Wrana, J. L., Nesvizhskii, A. I., Raught, B., Tyers, M., and Gingras, A. C. (2010) ProHits: integrated software for mass spectrometry-based interaction proteomics. *Nat. Biotechnol.* **28,** 1015–1017
26. Eng, J. K., Jahan, T. A., and Hoopmann, M. R. (2013) Comet: an open-source MS/MS sequence database search tool. *Proteomics* **13,** 22–24
27. Keller, A., Nesvizhskii, A. I., Kolker, E., and Aebersold, R. (2002) Empirical statistical model to estimate the accuracy of peptide identifications made by MS/MS and database search. *Anal. Chem.* **74,** 5383–5392
28. Nesvizhskii, A. I., Keller, A., Kolker, E., and Aebersold, R. (2003) A statistical model for identifying proteins by tandem mass spectrometry. *Anal. Chem.* **75,** 4646–4658
29. Breitkreutz, A., Choi, H., Sharom, J. R., Boucher, L., Neduva, V., Larsen, B., Lin, Z. Y., Breitkreutz, B.-J., Stark, C., Liu, G., Ahn, J., Dewar-Darch, D., Reguly, T., Tang, X., Almeida, R., Qin, Z. S., Pawson, T., Gingras, A. C., Nesvizhskii, A. I., and Tyers, M. (2010) A global protein kinase and phosphatase interaction network in yeast. *Science* **328,** 1043–1046
30. Teo, G., Liu, G., Zhang, J., Nesvizhskii, A. I., Gingras, A. C., and Choi, H. (2014) SAINTexpress: improvements and additional features in Significance Analysis of INTeractome software. *J. Proteomics* **100,** 37–43
31. Choi, H., Larsen, B., Lin, Z. Y., Breitkreutz, A., Mellacheruvu, D., Fermin, D., Qin, Z. S., Tyers, M., Gingras, A. C., and Nesvizhskii, A. I. (2011) SAINT: probabilistic scoring of affinity purification-mass spectrometry data. *Nat. Methods* **8,** 70–73
32. Mellacheruvu, D., Wright, Z., Couzens, A. L., Lambert, J. P., St-Denis, N. A., Li, T., Miteva, Y. V., Hauri, S., Sardiu, M. E., Low, T. Y., Halim, V. A., Bagshaw, R. D., Hubner, N. C., Al-Hakim, A., Bouchard, A., Faubert, D., Fermin, D., Dunham, W. H., Goudreault, M., Lin, Z. Y., Badillo, B. G., Pawson, T., Durocher, D., Coulombe, B., Aebersold, R., Superti-Furga, G., Colinge, J., Heck, A. J., Choi, H., Gstaiger, M., Mohammed, S., Cristea, I. M., Bennett, K. L., Washburn, M. P., Raught, B., Ewing, R. M., Gingras, A. C., and Nesvizhskii, A. I. (2013) The CRAPome: a contaminant repository for affinity purification-mass spectrometry data. *Nat. Methods* **10,** 730–736
33. Taipale, M., Tucker, G., Peng, J., Krykbaeva, I., Lin, Z. Y., Larsen, B., Choi, H., Berger, B., Gingras, A. C., and Lindquist, S. (2014) A quantitative chaperone interaction network reveals the architecture of cellular protein homeostasis pathways. *Cell* **158,** 434–448
34. Shannon, P., Markiel, A., Ozier, O., Baliga, N. S., Wang, J. T., Ramage, D., Amin, N., Schwikowski, B., and Ideker, T. (2003) Cytoscape: a software environment for integrated models of biomolecular interaction networks. *Genome Res.* **13,** 2498–2504
35. Knight, J. D., Liu, G., Zhang, J., Pasculescu, A., Choi, H., and Gingras, A.-C. (2014) A web-tool for visualizing quantitative protein–protein interaction data. *Proteomics* doi: 10.1002/pmic.20145308
36. Berger, P., Berger, I., Schaffitzel, C., Tersar, K., Volkmer, B., and Suter, U. (2006) Multi-level regulation of myotubularin-related protein-2 phosphatase activity by myotubularin-related protein-13/set-binding factor-2. *Hum. Mol. Genet.* **15,** 569–579
37. Kim, S. A., Vacratsis, P. O., Firestein, R., Cleary, M. L., and Dixon, J. E. (2003) Regulation of myotubularin-related (MTMR)2 phosphatidylinositol phosphatase by MTMR5, a catalytically inactive phosphatase. *Proc. Natl. Acad. Sci. U.S.A.* **100,** 4492–4497
38. Fabbro, M., Zhou, B. B., Takahashi, M., Sarcevic, B., Lal, P., Graham, M. E., Gabrielli, B. G., Robinson, P. J., Nigg, E. A., Ono, Y., and Khanna, K. K. (2005) Cdk1/Erk2- and Plk1-dependent phosphorylation of a centrosome protein, Cep55, is required for its recruitment to midbody and cytokinesis. *Dev. Cell* **9,** 477–488
39. Steigemann, P., and Gerlich, D. W. (2009) Cytokinetic abscission: cellular dynamics at the midbody. *Trends Cell Biol.* **19,** 606–616
40. Zhao, W. M., Seki, A., and Fang, G. (2006) Cep55, a microtubule-bundling protein, associates with centralspindlin to control the midbody integrity and cell abscission during cytokinesis. *Mol. Biol. Cell* **17,** 3881–3896
41. Sagona, A. P., Nezis, I. P., Pedersen, N. M., Liestøl, K., Poulton, J., Rusten, T. E., Skotheim, R. I., Raiborg, C., and Stenmark, H. (2010) PtdIns(3)P controls cytokinesis through KIF13A-mediated recruitment of FYVE-CENT to the midbody. *Nat. Cell Biol.* **12,** 362–371
42. Zhao, R., Qi, Y., and Zhao, Z. J. (2000) FYVE-DSP1, a dual-specificity protein phosphatase containing an FYVE domain. *Biochem. Biophys. Res. Commun.* **270,** 222–229
43. Zhao, R., Qi, Y., Chen, J., and Zhao, Z. J. (2001) FYVE-DSP2, a FYVE domain-containing dual specificity protein phosphatase that dephosphorylates phosphotidylinositol 3-phosphate. *Exp. Cell Res.* **265,** 329–338
44. Naughtin, M. J., Sheffield, D. A., Rahman, P., Hughes, W. E., Gurung, R., Stow, J. L., Nandurkar, H. H., Dyson, J. M., and Mitchell, C. A. (2010) The myotubularin phosphatase MTMR4 regulates sorting from early endosomes. *J. Cell Sci.* **123,** 3071–3083
45. Lorenzo, O., Urbé, S., and Clague, M. J. (2005) Analysis of phosphoinositide binding domain properties within the myotubularin-related protein MTMR3. *J. Cell Sci.* **118,** 2005–2012
46. Walker, D. M., Urbe, S., Dove, S. K., Tenza, D., Raposo, G., and Clague, M. J. (2001) Characterization of MTMR3 : an inositol lipid 3-phosphatase with novel substrate specificity. *Curr. Biol.* **11,** 1600–1605
47. Tsujita, K., Itoh, T., Ijuin, T., Yamamoto, A., Shisheva, A., Laporte, J., and Takenawa, T. (2004) Myotubularin regulates the function of the late endosome through the gram domain-phosphatidylinositol 3,5-bisphosphate interaction. *J. Biol. Chem.* **279,** 13817–13824
48. Wolf, E., Kim, P. S., and Berger, B. (1997) MultiCoil: a program for predicting two- and three-stranded coiled coils. *Protein Sci.* **6,** 1179–1189
49. Lee, H. H., Elia, N., Ghirlando, R., Lippincott-Schwartz, J., and Hurley, J. H. (2008) Midbody targeting of the ESCRT machinery by a noncanonical coiled coil in CEP55. *Science* **322,** 576–580
50. Golsteyn, R. M., Mundt, K. E., Fry, A. M., and Nigg, E. A. (1995) Cell cycle regulation of the activity and subcellular localization of Plk1, a human protein kinase implicated in mitotic spindle function. *J. Cell Biol.* **129,** 1617–1628

51. Hamanaka, R., Smith, M. R., O'Connor, P. M., Maloid, S., Mihalic, K., Spivak, J. L., Longo, D. L., and Ferris, D. K. (1995) Polo-like kinase is a cell cycle-regulated kinase activated during mitosis. *J. Biol. Chem.* **270,** 21086–21091
52. Guizetti, J., Schermelleh, L., Mäntler, J., Maar, S., Poser, I., Leonhardt, H., Müller-Reichert, T., and Gerlich, D. W. (2011) Cortical constriction during abscission involves helices of ESCRT-III-dependent filaments. *Science* **331,** 1616–1620
53. Elia, N., Fabrikant, G., Kozlov, M. M., and Lippincott-Schwartz, J. (2012) Computational model of cytokinetic abscission driven by ESCRT-III polymerization and remodeling. *Biophys. J.* **102,** 2309–2320
54. Elia, N., Sougrat, R., Spurlin, T. A., Hurley, J. H., and Lippincott-Schwartz, J. (2011) Dynamics of endosomal sorting complex required for transport (ESCRT) machinery during cytokinesis and its role in abscission. *Proc. Natl. Acad. Sci. U.S.A.* **108,** 4846–4851
55. Keller, D. M., Zeng, X., Wang, Y., Zhang, Q. H., Kapoor, M., Shu, H., Goodman, R., Lozano, G., Zhao, Y., and Lu, H. (2001) A DNA damage-induced p53 serine 392 kinase complex contains CK2, hSpt16, and SSRP1. *Mol. Cell* **7,** 283–292
56. Keller, D. M., and Lu, H. (2002) p53 serine 392 phosphorylation increases after UV through induction of the assembly of the CK2.hSPT16.SSRP1 complex. *J. Biol. Chem.* **277,** 50206–50213
57. Zhang, M., Han, G., Wang, C., Cheng, K., Li, R., Liu, H., Wei, X., Ye, M., and Zou, H. (2011) A bead-based approach for large-scale identification of *in vitro* kinase substrates. *Proteomics* **11,** 4632–4637
58. Vinayagam, A., Stelzl, U., Foulle, R., Plassmann, S., Zenkner, M., Timm, J., Assmus, H. E., Andrade-Navarro, M. A., and Wanker, E. E. (2011) A directed protein interaction network for investigating intracellular signal transduction. *Sci. Signal* **4,** rs8
59. Cuadrado, A., Lafarga, V., Cheung, P. C., Dolado, I., Llanos, S., Cohen, P., and Nebreda, A. R. (2007) A new p38 MAP kinase-regulated transcriptional coactivator that stimulates p53-dependent apoptosis. *EMBO J.* **26,** 2115–2126
60. Alvarez-Venegas, R., Sadder, M., Hlavacka, A., Baluska, F., Xia, Y., Lu, G., Firsov, A., Sarath, G., Moriyama, H., Dubrovsky, J. G., and Avramova, Z. (2006) The Arabidopsis homolog of trithorax, ATX1, binds phosphatidylinositol 5-phosphate, and the two regulate a common set of target genes. *Proc. Natl. Acad. Sci. U.S.A.* **103,** 6049–6054
61. Elia, A. E., Cantley, L. C., and Yaffe, M. B. (2003) Proteomic screen finds pSer/pThr-binding domain localizing Plk1 to mitotic substrates. *Science* **299,** 1228–1231
62. Elia, A. E., Rellos, P., Haire, L. F., Chao, J. W., Ivins, F. J., Hoepker, K., Mohammad, D., Cantley, L. C., Smerdon, S. J., and Yaffe, M. B. (2003) The molecular basis for phosphodependent substrate targeting and regulation of Plks by the Polo-box domain. *Cell* **115,** 83–95
63. Cheng, K. Y., Lowe, E. D., Sinclair, J., Nigg, E. A., and Johnson, L. N. (2003) The crystal structure of the human polo-like kinase-1 polo box domain and its phospho-peptide complex. *EMBO J.* **22,** 5757–5768
64. Fujiwara, T., Bandi, M., Nitta, M., Ivanova, E. V., Bronson, R. T., and Pellman, D. (2005) Cytokinesis failure generating tetraploids promotes tumorigenesis in p53-null cells. *Nature* **437,** 1043–1047
65. Ganem, N. J., Storchova, Z., and Pellman, D. (2007) Tetraploidy, aneuploidy, and cancer. *Curr. Opin. Genet. Dev.* **17,** 157–162
66. Steigemann, P., Wurzenberger, C., Schmitz, M. H., Held, M., Guizetti, J., Maar, S., and Gerlich, D. W. (2009) Aurora B-mediated abscission checkpoint protects against tetraploidization. *Cell* **136,** 473–484
67. Smith, M. R., Wilson, M. L., Hamanaka, R., Chase, D., Kung, H., Longo, D. L., and Ferris, D. K. (1997) Malignant transformation of mammalian cells initiated by constitutive expression of the polo-like kinase. *Biochem. Biophys. Res. Commun.* **234,** 397–405
68. Medema, R. H., Lin, C. C., and Yang, J. C. (2011) Polo-like kinase 1 inhibitors and their potential role in anticancer therapy, with a focus on NSCLC. *Clin. Cancer Res.* **17,** 6459–6466
69. Tao, J., Zhi, X., Tian, Y., Li, Z., Zhu, Y., Wang, W., Xie, K., Tang, J., Zhang, X., Wang, L., and Xu, Z. (2014) CEP55 contributes to human gastric carcinoma by regulating cell proliferation. *Tumour Biol.* **35,** 4389–4399
70. Chen, C. H., Lu, P. J., Chen, Y. C., Fu, S. L., Wu, K. J., Tsou, A. P., Lee, Y. C., Lin, T. C., Hsu, S. L., Lin, W. J., Huang, C. Y., and Chou, C. K. (2007) FLJ10540-elicited cell transformation is through the activation of PI3-kinase/AKT pathway. *Oncogene* **26,** 4272–4283
71. Hanahan, D., and Weinberg, R. A. (2000) The hallmarks of cancer. *Cell* **100,** 57–70